Ground states of a two-dimensional frustrated quantum antiferromagent Cs_2CuCl_4

by

Younghyun Kim

Submitted to the Department of Physics
in partial fulfillment of the requirements for the degree of

Bachelor of Science in Physics

at the

MASSACHUSETTS INSTITUTE OF TECHNOLOGY

June 2008

Author .....
.....
Department of Physics
April 17, 2008

Certified by....
.....
Professor Xiao-Gang Wen
Department of Physics
Thesis Supervisor

Accepted by.....
.....
Professor David Pritchard
Senior Thesis Coordinator, Department of Physics

Ground states of a two-dimensional frustrated quantum antiferromagent Cs_2CuCl_4

by

Younghyun Kim

Submitted to the Department of Physics
on April 17, 2008, in partial fulfillment of the
requirements for the degree of
Bachelor of Science in Physics

Abstract

The properties of a frustrated quantum antiferromagnet are interesting topics in condensed matter theory. Among the quantum antiferromagnets, Cs_2CuCl_4 gains attention as one of the candidates for materials with ground state spin liquid phase. The recent experimental results show that there exist several ground state phases in the presence of magnetic field which cannot be explained with classical Hamiltonian. In the thesis, I numerically studied the ground state of Cs_2CuCl_4 using a modified classical Hamiltonian, and I compared the result with previous experiments and classical analysis. The resulted magnetic phase diagram contains two phases, cone and ferromagnetic phase, which are separated by second order transition and a first order transition line for intermediate longitudinal field which ends up with a critical point.

Thesis Supervisor: Professor Xiao-Gang Wen
Title: Department of Physics

Acknowledgments

I want to express my sincere gratitude to professor Xiao-Gang Wen for all the helpful advice and opportunities he has given me during my undergraduate years at MIT. I personally owe so much to him, ranging from the statistical physics class to my undergraduate research experience. I greatly enjoyed them, and those experiences are the most valuable academic inspiration in my times at MIT.

I want to thank Bruce Knuteson who was my academic advisor during the last three years and who gave me great advice on my course choices, research experiences and school life in general.

I would like to give special thanks to professor Patrick Lee and other professors of physics department for the deep and wide academic experiences I got from their exciting classes. I also thanks to Ying Ran for helpful comments regarding my research. I could not make a great progress during the last summer without his help.

I want to thank my family for supporting me always that I could get to here today. Finally I would like to thank my friends here at MIT for making my time at MIT unforgettable.

Contents

List of Figures

Chapter 1

Introduction

The modern condensed matter physics deals with many exciting phenomena in huge range of materials with many-body systems. Among them, the frustrated quantum antiferromagnet becomes a hot material in experimental and theoretical researches because of its potential of having strong quantum fluctuation which leads to exotic spin-liquid ground states.[1][10] Especially, the quantum antiferromagnet Cs_2CuCl_4, which has spin-1/2 triangular spin lattice structure, gains lots of attention as a candidate for such material. In several published result of inelastic neutron scattering experiments on Cs_2CuCl_4, a broad continuum is observed,[8] and one of the explanations for this continuum uses spin-liquid states.[3][4][14] As well as the spin liquid states of Cs_2CuCl_4, the low-temperature states of Cs_2CuCl_4 in the presence of magnetic field also have interesting aspects. The low-temperature states depend on the strength and direction of magnetic field. The states with three directions of magnetic field are studied separately. One is a direction perpendicular to the plane of triangular lattice, marked by a, and the other two directions are within the plane of lattice, marked by b and c. With the magnetic field in a-direction, there is a phase transition at the critical field of $B^a_{cr} = 8.44$T.[7] The phase with magnetic field less than B^a_{cr} is a cone phase. For the stronger field, the magnetization is saturated and every spin vector point the direction of magnetic field.[7] The phases with magnetic field within b-c plane are more complicated, so they will be discussed later. There are some recent efforts to understand the nature of these phases theoretically. Some

phases of ground states of Cs_2CuCl_4 in the magnetic field can be understood using a semi-classical method which includes quantum fluctuation effect.[13]

However, the result of semi-classical method still cannot explain several phases with intermediate field in b-c plane. Moreover, the differences between phase diagrams for magnetic fields in b-direction and c-direction cannot be explained by semi-classical analysis. In understanding the nature of this difference, difference between phase diagrams in different directions, the phase diagram for magnetic field in all direction can be a strong tool. When we can determine the phases for all $\vec{B} = (B^a, B^b, B^c)$, we may predict the reason for this difference easily. However, the phase diagram for low-temperature states in the presence of magnetic field in out of axis direction is not constructed yet. To resolve this problems, I will introduce the numerical method I used to find the ground state phase diagram of Cs_2CuCl_4 with an abstract magnetic field $\vec{B} = (B^a, 0, B^c)$. I will also report the resulting phase diagram and analyze the result.

In Chapter 2, I will describe the crystal structure and spin Hamiltonian of Cs_2CuCl_4. The classical analysis will be introduced in Chapter 3. Chapter 4 contains the main result of this paper. I will introduce the models I used for the numerical calculation and corresponding results in Chapter 4. Analysis of the results with order parameters will be illustrated in this chapter too. Chapter 5 will give a summary of the result.

Chapter 2

Properties of Cs_2CuCl_4

2.1 Crystal Structure of Cs_2CuCl_4

The crystal structure of Cs_2CuCl_4 is described in Figure 2-1.[8] It is orthorhombic structure with lattice parameters at 0.3 K of $a = 9.65$Å, $b = 7.48$Åand $c = 12.26$Å, and consists of $CuCl_4^{2-}$ tetrahedra arranged in layers separated in a-direction.[6] The magnetic moments are carried by Cu^{2+} ions in tetrahedra. Each Cu^{2+} ion carries a spin of 1/2. The magnetic sites in a single layer is shown in Figure 2-2.[13] As it is shown in the figure, the magnetic moments of Cs_2CuCl_4 form a triangular lattice with exchange interactions. Because of the geometric effects, this triangular lattice has a anisotropic property. The exchange interactions with parameter J along the same chain, which is parallel to b-direction, are larger than exchange interactions between the adjacent chains J'.[7] There are also interlayer exchange interactions between nearest neighbors. However, the previous experiments by Coldea et al[6] shows that this interlayer interactions are far weaker than the in-plane couplings. Therefore, we can consider Cs_2CuCl_4 as a quasi-2D low-exchange quantum magnet.[8]

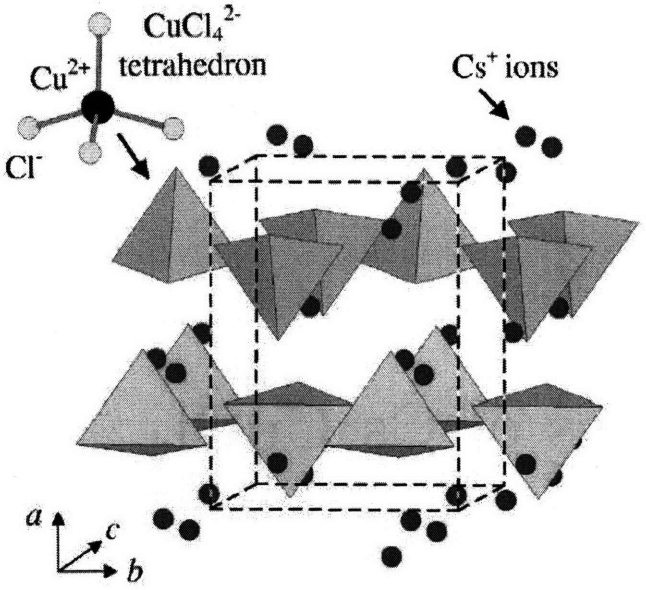

Figure 2-1: Crystal Structure of Cs_2CuCl_4[8]

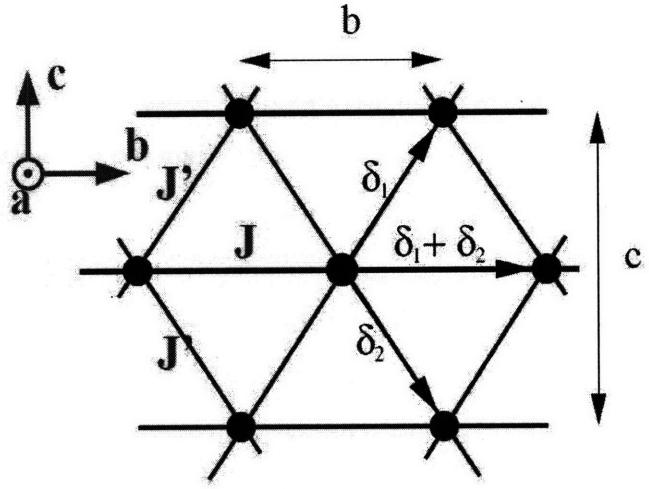

Figure 2-2: Magnetic sites with couplings in a single layer of Cs_2CuCl_4[13]

2.2 Experimental Results

Several experiments for determining the B-T phase diagram of Cs_2CuCl_4 in low temperature were made.[7][6][12] The experimental results for determining magnetic phase diagram in the magnetic field along the a axis were given in the references [6] and [12].

The Figure 2-3[12] shows that one phase transition appears in the experimental data for the magnetization. The solid lines are experimental data, and the dashed,

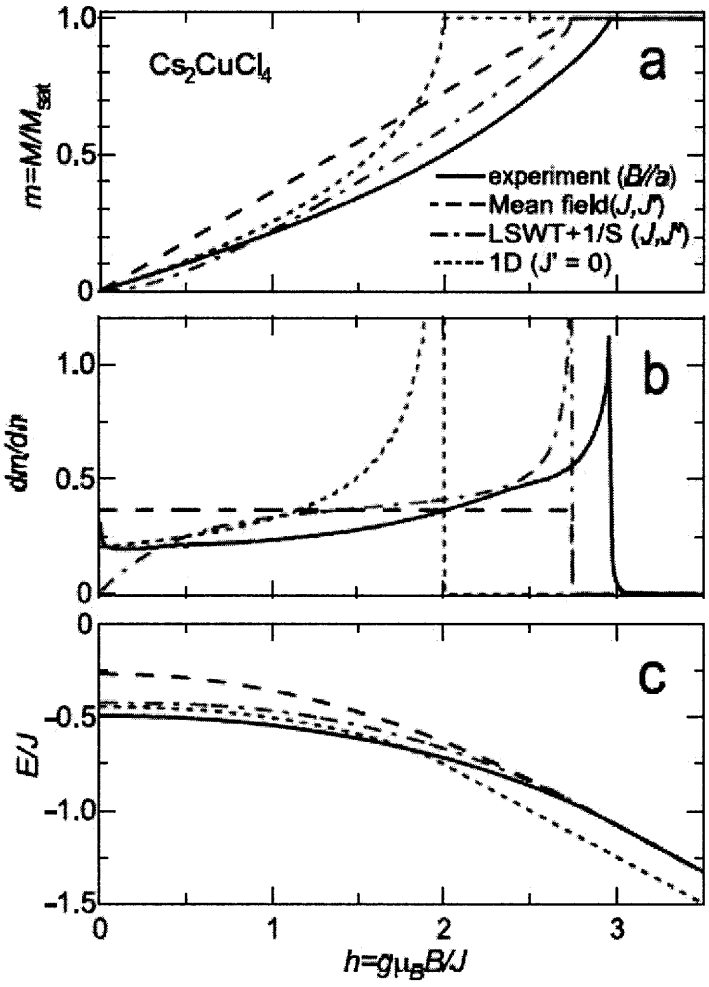

Figure 2-3: (a)Reduced Magnetization, (b)susceptibility, and (c)ground state energy of Cs_2CuCl_4 vs reduced field along the a-axis.[12]

dash-dotted and dotted lines are semi classical mean-field prediction, linear spin-wave theory with 1st order quantum corrections and Bethe-ansatz prediction for 1D chains

along the b-axis.[12]

The results of neutron scattering experiment performed by Coldea et al.[6] suggests that the phase transition for the magnetic field along the a-axis appears at the critical field B_c = 8.44(1) T. The Figure 2-4[6] shows the results of this experiment. The

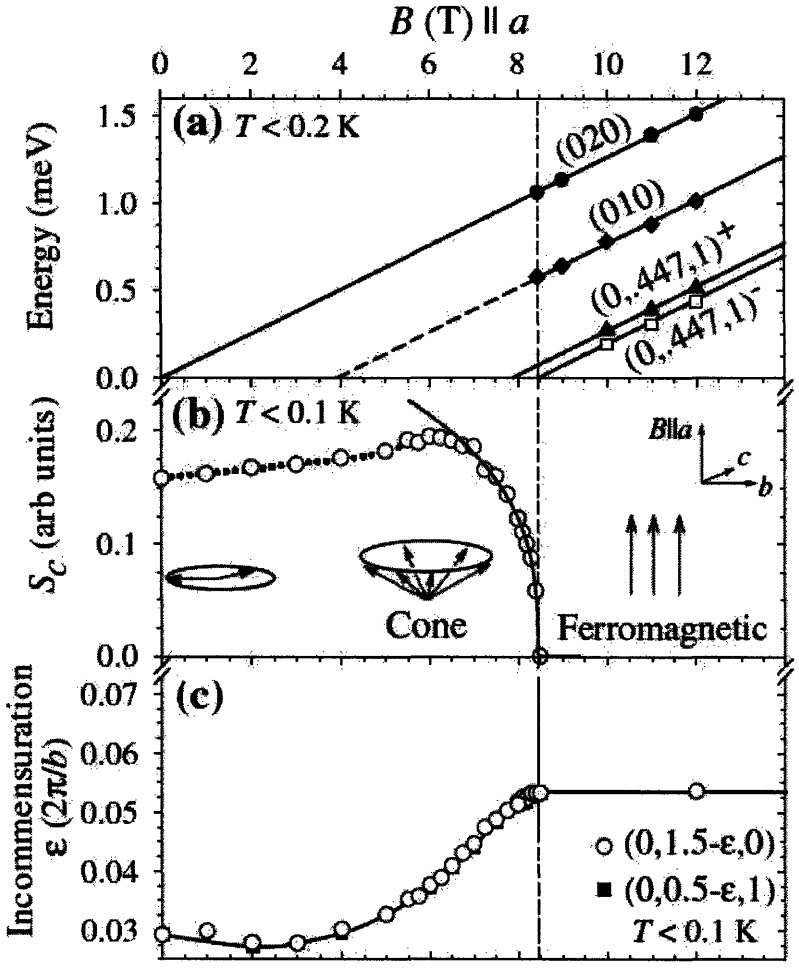

Figure 2-4: (a)Magnon energies, (b)amplitude of perpendicular ordered moment S_c, and (c)Incommensuration vs field along the a-axis.[6]

measured spin order forms an elliptical cone phase below the critical field.

$$\vec{S_R} = S_b \cos \vec{Q} \cdot \vec{R}\hat{b} + S_c \sin \vec{Q} \cdot \vec{R}\hat{c} + S_a \hat{a} \tag{2.1}$$

$\vec{Q}$ denotes the wavevector of the spin wave which is made by projection of the cone into the b-c plane. $\vec{R}$ indicates the location vector of each spin. Above the critical

field, every spin point the direction of magnetic field, and ferromagnetic property appears.[6] Resulting B-T phase diagram is illustrated in Figure 2-5[7]. The square

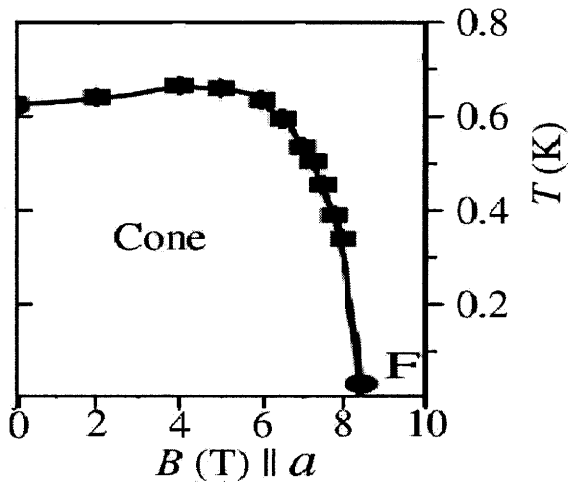

Figure 2-5: B-T phase diagram of Cs_2CuCl_4 in a field along the a-axis. [7]

points are the data from neutron scattering[6][5], and the circle point is from the susceptibility.[12]

The magnetic phase of Cs_2CuCl_4 for the field along the b and c axes are more complicated. The magnetic phase diagram of Cs_2CuCl_4 with the magnetic field along the b and axes is studied using the magnetization curves of Cs_2CuCl_4.

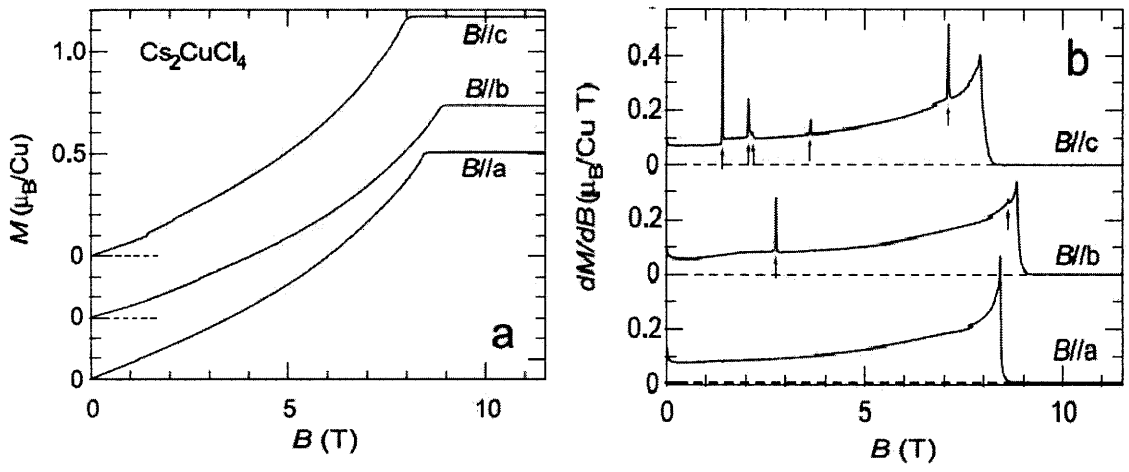

Figure 2-6: (a)Magnetization and (b)susceptibility of Cs_2CuCl_4 vs fields along the directions of axes. [12]

As we can see in the plot of susceptibility vs magnetic field in Figure 2-6, several

phase transitions of Cs_2CuCl_4 in the magnetic field along the b and c axes were discovered. The vertical arrows in the susceptibility curves indicate the points of phase transition. The temperature condition is 0.05K for the curves with field along the a and b axes and 0.07K for the curve with field along the c axis. The reported value of the critical field for saturation is $B_{cr}^a = 8.44(2)$, $B_{cr}^b = 8.89(2)$ and $B_{cr}^c = 8.00(2)$.[12] Above this critical field, paramagnetic phase appears. The collected result of B-T phase diagram for the magnetic field in b-c plane is described in Figure 2-7.[12] The "Spiral" on the phase diagram denotes the planar spin wave phase where every spin vector is in b-c plane with spin wavevector $\vec{Q}$ which appeared in the equation (2.1). "E" on the phase diagram for the field along the c-axis indicates the elliptical phase. This phase appears for 1.4 T $<$ B^c $<$ 2.1 T. In the elliptical phase, the structure of the spin vectors has elliptical shape with large elongation along the c-axis.[7] For the field along the b-axis, this elliptical phase does not appear, and the system evolves from spiral phase to a phase without long-range order. In the case of magnetic phase diagram for the field along the c-axis, the system does not have any long-range order for the magnetic field above 2.1 T and the system is in a spin liquid state.[7]. The appearance of the phases in this range of field cannot be explained with semi-classical analysis. Further experiment with neutron scattering method may tell us the magnetic properties of these phases. The appearance of spiral and elliptical phases are explained with semi-classical method including the quantum fluctuation effect.[13] I will discuss the theoretical calculation by introducing spin Hamiltonian in the next section. In the strong field limit, $B > B_{cr}$, both phases with the field along b and c axes evolve into a paramagnetic phase.

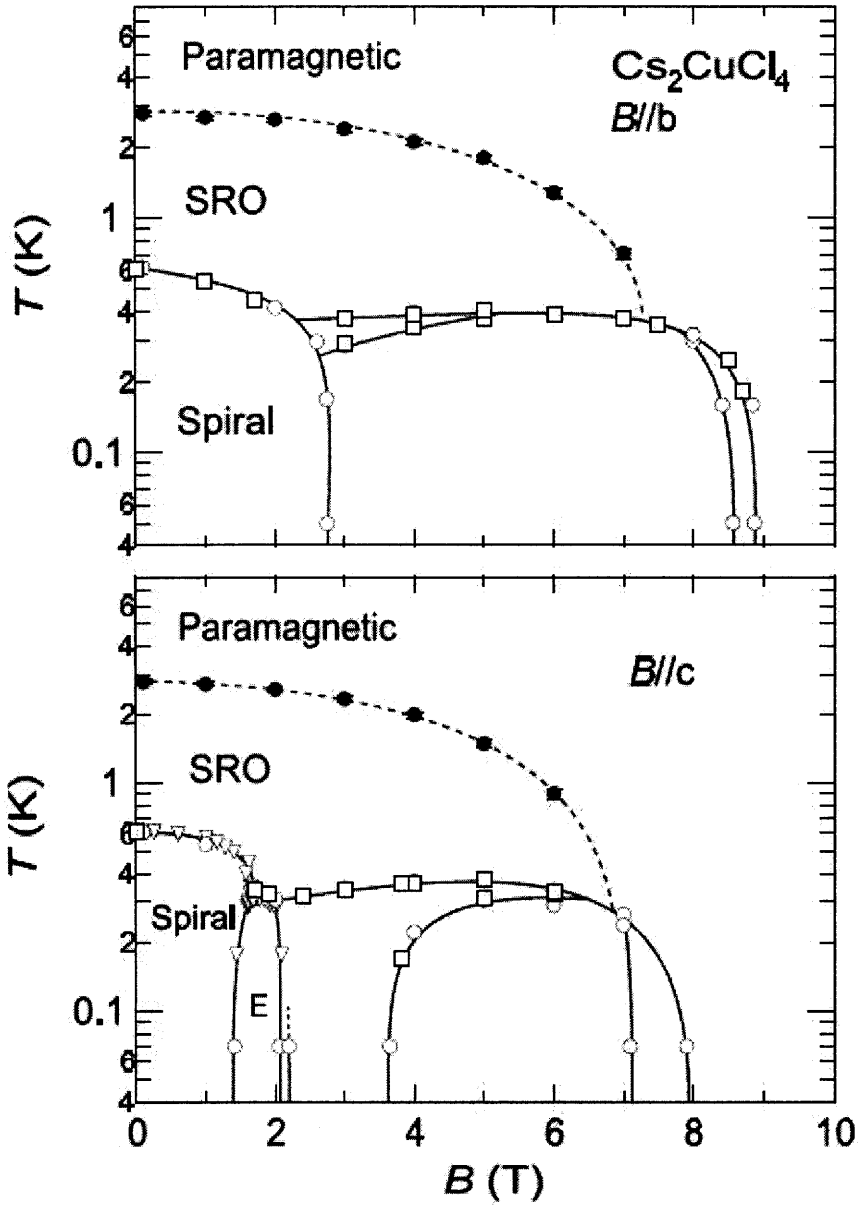

Figure 2-7: B-T phase diagram of Cs_2CuCl_4 for the field along the b and c axes.[12]

2.3 The Spin Hamiltonian of Cs_2CuCl_4

In classical model, the spin Hamiltonian of Cs_2CuCl_4 consists of three parts as following.

$$\mathcal{H} = \mathcal{H}_0 + \mathcal{H}_{DM} + \mathcal{H}_B \tag{2.2}$$

$\mathcal{H}_0$ is the Heisenberg exchange energy and can be expressed as following equation.[13]

$$\begin{aligned} \mathcal{H}_0 = \sum_R \quad & [J\vec{S}_R \cdot \vec{S}_{R+\delta_1+\delta_2} \\ & + J'(\vec{S}_R \cdot \vec{S}_{R+\delta_1} + \vec{S}_R \cdot \vec{S}_{R+\delta_2}) \\ & + J''\vec{S}_R \cdot \vec{S}_{R+\delta_3}] \end{aligned} \tag{2.3}$$

The vectors δ_1 and δ_2 are same as vectors in the Figure 2-2[13]. The other vector δ_3 is an out of plane vector between the spins on adjacent layers. R is a position vector for each site. Therefore, the first term in the equation (2.3) denotes the exchange interaction between spins on the same chain along the b-axis. The second term represents the interaction between spins on adjacent chains. The last term of the equation demonstrates the weak interlayer interactions between spins on adjacent layers. The values of parameters, J, J' and J'' depend on the applied magnetic field. For a strong field, their values were determined experimentally. Their values at $B^a = 12T$ are 0.374(5), 0.128(5) and 0.017(2) meV respectively.[6] The interlayer interaction is very small when compared to inplane interactions. One can directly find that the Heisenberg exchange Hamiltonian is perfectly symmetric in 3D and, as a result, has SU(2) symmetry which means that energy does not change when we rotate every spin by same angle in any direction.

The second term of the equation (2.2) is called Dzyaloshinskii-Moriya(DM) interaction. [9][11] The energy for the DM interaction is given by

$$\mathcal{H}_{DM} = -\sum_R (-1)^n \vec{D} \cdot \vec{S}_R \times [\vec{S}_{R+\delta_1} + \vec{S}_{R+\delta_2}], \tag{2.4}$$

where $\vec{D} = (D, 0, 0)$ is associated with the oriented bond between the coupled spins.[13]

The value $D = 0.020(2)$ meV is acquired experimentally.[7] The presence of the DM interaction makes spins prefer to lie on b-c plane because the direction of $\vec{D}$ is the along the a-axis. Also the inclusion of DM interaction reduces the spin symmetry. Since $\vec{D}$ is in a-axis, $\mathcal{H}_{DM}$ contains rotation symmetry about a-axis. However, there is no spherical rotation symmetry anymore. The DM interaction allows $\mathbb{Z}_2$ symmetry since it does not change when we change the sign of the each component of a spin. Therefore, the DM interaction reduces spin symmetry of the Hamiltonian from SU(2) to $\mathbb{Z}_2 \otimes$ U(1). In the factor $(-1)^n$, n denotes the layer index, and this factor makes the sign of DM interaction alternates between odd and even layers. Another important aspect of the DM interaction is that it prefers specific chirality of the spin order. When two nearest spin vectors in b-c plane separated by δ_1 have angle difference θ, the presence of the DM interaction decides the spin which has to have larger angle. This chirality becomes a important factor when we decide a sign of the wavevector of spin wave in the next chapter.

The last term of the Hamiltonian is the Zeeman energy which is given by

$$\mathcal{H}_B = -\sum_R g_i \mu_B B^i S_R^i, \tag{2.5}$$

in a magnetic field $\vec{B} = (B^a, B^b, B^c)$.[13] g_i is the gyromagnetic tensor $g = (2.20, 2.08, 2.30)$. [2] This term in the spin Hamiltonian makes spins like to lie along the direction of the magnetic field. As a result, paramagnetic phase appears for the strong magnetic field. The presence of magnetic field breaks symmetry again. When we apply a field along a-axis, it breaks the $\mathbb{Z}_2$ symmetry and reduces the symmetry to U(1). When we put a field in b-c plane, it breaks U(1) symmetry, and the spin symmetry becomes $\mathbb{Z}_2$.

Chapter 3

Classical Analysis

The classical analysis of the ground states of Cs_2CuCl_4 starts from the spin Hamiltonian in equation(2.2)[13]. For the simplicity, I will neglect the interlayer interactions since the magnitude of interlayer interactions with parameter J'' is much smaller than that of the in-plane exchange interactions with parameter J and J'.[6] Since the Hamiltonian parameters J, J' and D may depend on the magnetic field, I used their ratios at $B^a = 12T$[7] for the analysis. In this chapter, I will discuss the classical analysis of the ground states of Cs_2CuCl_4 without external magnetic field first. Then I will expand our analysis into the ground states with a magnetic field.

3.1 The Ground State of Cs_2CuCl_4 in the Absence of Magnetic Field

When there is no magnetic field in the system, we can eliminate the Zeeman energy term from the equation(2.2)[13]. The resulting Hamiltonian has following shape.

$$\begin{aligned}\mathcal{H} = \sum_R \quad & [J\vec{S}_R \cdot \vec{S}_{R+\delta_1+\delta_2} \\ & +J'(\vec{S}_R \cdot \vec{S}_{R+\delta_1} + \vec{S}_R \cdot \vec{S}_{R+\delta_2}) \\ & -(-1)^n \vec{D} \cdot \vec{S}_R \times [\vec{S}_{R+\delta_1} + \vec{S}_{R+\delta_2}]]\end{aligned} \tag{3.1}$$

From now on, I will set $n = 0$ for the simplicity of expressions.

The Figure 3-1 shows the unit cell of the anisotropic triangular lattice of Cs_2CuCl_4. Black points denote the spin sites. The paths for the exchange interactions of the unit cell are drawn with solid line. Each of the four points in the unit cell has its dimensionless site vector marked by R_n. The DM interaction favors state in which

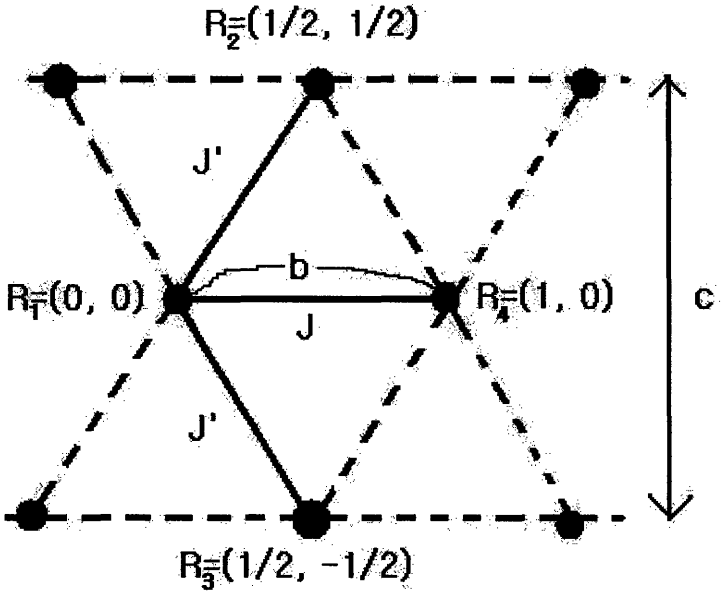

Figure 3-1: The unit cell and interaction paths of the triangular spin lattice of Cs_2CuCl_4.

spins lie in the b-c plane as we have mentioned above. Since there is no preferred direction of spin vectors in $\mathcal{H}_0$ of equation (2.4), without magnetic field, every spin lies in b-c plane because of the DM interaction. Since the spin system has U(1) symmetry and every spin sites are isotropic, we can assume that the spins have spin wave structure with some wavevector $\vec{Q} = (Q_b, Q_c)$. Thus the assumed model for the spin configuration can be written as follow.

$$\vec{S_R} = S(\cos(\vec{Q} \cdot \vec{R} + \alpha)\hat{b} + \sin(\vec{Q} \cdot \vec{R} + \alpha)\hat{c}) \tag{3.2}$$

S is the length of a spin $S = 1/2$. Here, we can make a prediction on $\vec{Q}$. Since the triangular lattice plane has symmetry against the b-axis, $Q_c = 0$ is expected for the ground state. The Figure 3-2 shows the spin configuration for the ground state of the

model with $Q_b = \pi/3$ and $Q_c = 0$ in the absence of a magnetic field.

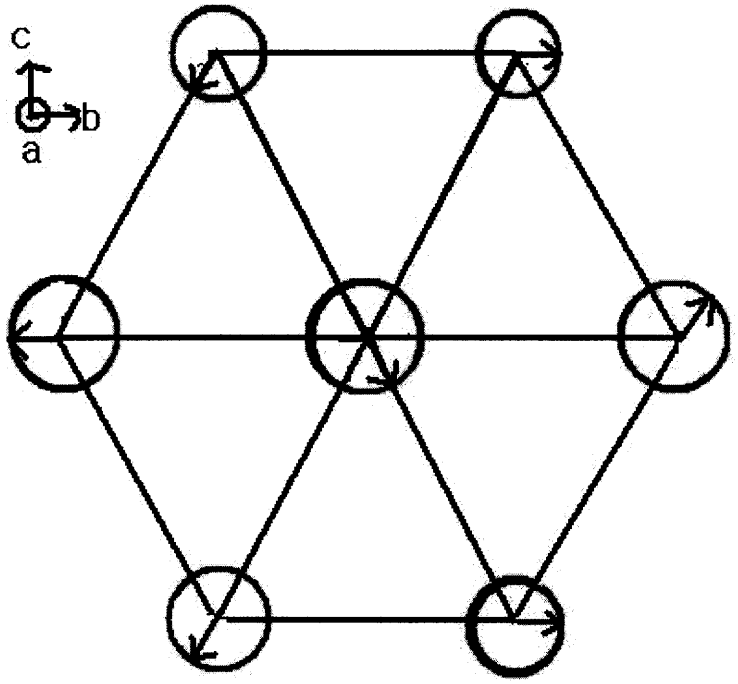

Figure 3-2: The spin configuration of the classical model without magnetic field.

The energy of the unit cell can be derived directly by putting (3.2) into the Hamiltonian. With set up of $\alpha = 0$ and choices of $\vec{R}$s as in Figure 3-1, energy can be written as follow.

$$\begin{aligned} E &= \frac{1}{4}J\cos(Q_b) + \frac{1}{4}J'\left(\cos\left(\frac{Q_b}{2}+\frac{Q_c}{2}\right)+\cos\left(\frac{Q_b}{2}-\frac{Q_c}{2}\right)\right) \\ &\quad -\frac{1}{4}D\left(\sin\left(\frac{Q_b}{2}+\frac{Q_c}{2}\right)+\sin\left(\frac{Q_b}{2}-\frac{Q_c}{2}\right)\right) \end{aligned} \tag{3.3}$$

The factor $\frac{1}{4}$ is from the square of the length of a spin $S = 1/2$. Minimizing this function of Q with reported ratios of J, J' and D[6][7] gives $Q_b = 3.48$ and $Q_c = 0$. As expected already, the wavevecotr of spin wave $\vec{Q}$ is along the b-axis. This quantity means that two spins on sites separated by distance nb, where b is the spacing of lattice in b-axis, in b direction have angle difference of $n \times 3.48$ radian.

3.2 The Ground State of Cs_2CuCl_4 in a Transverse Magnetic field

In the presence of a transverse field along the a-axis, spin Hamiltonian becomes

$$\begin{aligned}\mathcal{H} = \sum_R \quad & [J\vec{S}_R \cdot \vec{S}_{R+\delta_1+\delta_2} \\ & + J'(\vec{S}_R \cdot \vec{S}_{R+\delta_1} + \vec{S}_R \cdot \vec{S}_{R+\delta_2}) \\ & - \vec{D} \cdot \vec{S}_R \times [\vec{S}_{R+\delta_1} + \vec{S}_{R+\delta_2}] \\ & - g_a \mu_B B^a S^a_R]. \end{aligned} \tag{3.4}$$

Since the presence of a field along the a-axis does not break U(1) symmetry, the projection of the spins onto the b-c plane stays same. However, a magnetic field favors spins along the direction of the field. Therefore the result configuration becomes a cone with its axis pointing a-axis. This cone state can be written as follow.

$$\vec{S_R} = \frac{1}{2}(\cos\theta \hat{a} + \sin\theta \cos(\vec{Q} \cdot \vec{R})\hat{b} + \sin\theta \sin(\vec{Q} \cdot \vec{R})\hat{c}) \tag{3.5}$$

Here, $\hbar/2\cos\theta$ is the height of a cone. In this state, spin directions at different sites form a cone with its axis pointing a-axis. The value of θ can be expressed by a function of B^a when we minimize the following unit cell energy in (3.6).

$$\begin{aligned} E \;=\; & \frac{1}{4}J\sin^2\theta\cos(Q_b) + \frac{1}{4}J'\sin^2\theta\left(\cos\left(\frac{Q_b}{2}+\frac{Q_c}{2}\right)+\cos\left(\frac{Q_b}{2}-\frac{Q_c}{2}\right)\right) \\ & -\frac{1}{4}D\sin^2\theta\left(\sin\left(\frac{Q_b}{2}+\frac{Q_c}{2}\right)+\sin\left(\frac{Q_b}{2}-\frac{Q_c}{2}\right)\right) - \frac{1}{2}g_a\mu_B B^a\cos\theta \end{aligned} \tag{3.6}$$

Since the addition of $\sin\theta$ term does not change the dependence of energy on $\vec{Q}$, the value of $\vec{Q}$ stays same as in plane phase. Minimizing this equation for θ gives,

$$\cos\theta = -\frac{g_a\mu_B B^a}{J\cos Q_b + 2J'\cos\frac{Q_b}{2} - 2D\sin\frac{Q_b}{2}}. \tag{3.7}$$

However, this classical result does not agree nicely with experimental results. The disagreement is described in the Figure 2-3 (a). The dashed line marked by "Mean field" represents this classical result where the magnetization($\propto \cos\theta$) is proportional to B^a. For more accurate calculation, we have to use a Hamiltonian with quantum effects.[7] The exact treatment of the quantum Hamiltonian gives $B^a_{cr} = 8.36T$[6] where the reported experimental result is 8.44T. The small difference between these values are due to the neglected interlayer interaction. Since there is a large difference between the classical result (3.7) and experimental results, the absolute value of critical field strength is meaningless in classical calculation. Therefore, in the rest of this paper, I will use the notation h^i for the renormalized field $h^i = B^i/B^i_{cr}$ where B^i_{cr}s are the field strengths where the ferromagnetic states appear.

3.3 The Ground State of Cs_2CuCl_4 in a Longitudinal Magnetic Field

The ground state of Cs_2CuCl_4 with a longitudinal field shows more complexity than the ground state with a transverse field. There is no simple model which agrees well with experimental results for all range of field $0 < h < 1$. However, the tilted cone approximation gives a good agreement with numerical calculation.[13]

$$\begin{aligned} \vec{S_R} = \frac{1}{2} \; [\; & (\sin\theta\cos(\vec{Q}\cdot\vec{R})\cos\eta + \cos\theta\sin\eta)\hat{a} \\ & + \sin\theta\sin(\vec{Q}\cdot\vec{R})\hat{b} \\ & + (\cos\theta\cos\eta - \sin\theta\cos(\vec{Q}\cdot\vec{R})\sin\eta)\hat{c}] \end{aligned} \tag{3.8}$$

Vector (3.9) represents a cone spin configuration which tilted at an angle η to the c-axis and has a height $\cos\theta/2$. The more detailed analysis of spin configuration with classical Hamiltonian with a longitudinal field will be discussed with results of numerical calculation in the next chapter.

Chapter 4

Numerical Calculation

To investigate the ground state structure of Cs_2CuCl_4 in the presence of magnetic field in all direction, I calculated spin configurations by minimizing classical energy functions with or without quantum fluctuation effect. The system used in numerical analysis consists of 100 unit cells, 10 by 10 spin lattice, with open boundary condition. For the Hamiltonian, I chose the ratios $J/J' = 2.92$ and $D/J' = 0.156$ which are based on the experimental results in a strong magnetic field.[6] I neglected the interlayer interactions. Since the classical energy functions still have a U(1) symmetry with a magnetic field along a-axis, the spin configurations with B^a and B^b can represent all spin configurations with magnetic fields in any directions. Although there is a slight difference in scales because of the gyromagnetic tensor, the basic spin configuration phase diagrams become identical to the B^a-B^b phase diagram after a renormalization. Therefore, I chose the free B^a and B^b as variables used to investigate spin structure and axes for the resulted phase diagram.

4.1 Ground State Spin Configuration of Cs_2CuCl_4 in Classical Model

First, I numerically obtained spin configurations with classical model which fixes a spin length $S = 1/2$. The results of the numerical calculation is illustrated in the

phase diagram in Figure 4-1 There are two main phases in the spin configuration for

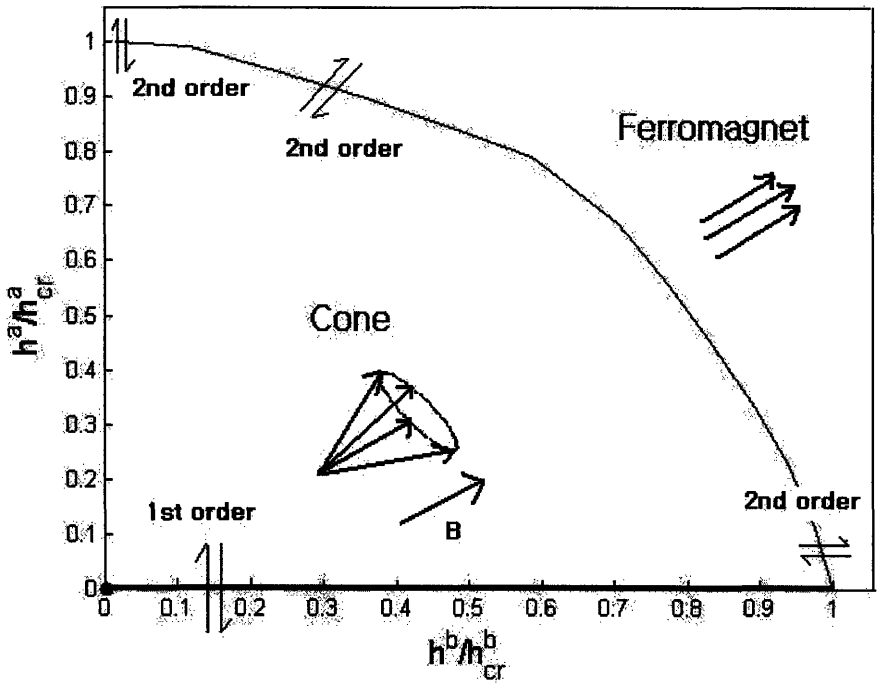

Figure 4-1: B^a-B^b phase diagram of the ground state of Cs_2CuCl_4 derived by numerical calculation without including quantum fluctuation effects

the ground state of Cs_2CuCl_4 with fixed spin length. For a strong magnetic field in any direction, every spin lie along the direction of the applied magnetic field and a ferromagnetic property appears. For a weak field, a tilted cone phase discussed in Section 3.3 appears. In the field along the a-direction, the axis of this cone points at the a-direction and its height which is correspond to a magnetization is proportional to the applied magnetic field. The transition from the ferromagnetic phase to the tilted cone phase is second order transition and breaks the translation symmetry of ferromagnetic phase. However, with a field purely in b-direction, the axis of the cone does not point at b-axis. It has a small angle η to b-axis as described in equation (3.9). This is a result of DM interaction which prefers spiral projection of spins into the b-c plane. The direction of the tiltedness can be $\hat{a}$ or $-\hat{a}$ with $B^a = 0$. Therefore, $\mathbb{Z}_2$ symmetry is broken in this region. However, when we add B^a too, the side in which a cone is tilted is decided by a sign of B^a. As a results, there is a jump in the function of $\eta(B^a)$ across the line $B^a = 0$, or b-axis as marked by thick solid line in Figure 4-1.

Above the b-axis, η has positive value and below the b-axis, η has negative value. In contrast, the axis of a cone changes smoothly cross the a-axis. The field strengths at the phase boundary h^a_{cr} and h^b_{cr} have ratio $h^b_{cr}/h^a_{cr} = 1.05$ which is consistent with the ratio of the components of the gyromagnetic tensor, $g^a/g^b = 1.06$.[2] The ratio from the experimental result is $8.89(T)/8.44(T) = 1.05$.

The spiral or distorted cycloid, planar phase which appeared for small B^b and $B^a = 0$ in previous experiment[12] and numerical calculation[13] does not appear in this model. To investigate the planar spin configuration, change of the length of spin by quantum fluctuation is required.

4.2 Ground State Spin Configuration of Cs_2CuCl_4 in Classical Model with Quantum Fluctuations

The effect of quantum fluctuations can be approximately represented by simply adding a term $\alpha(S - |\vec{S}|^2)^2$ to the Hamiltonian in equation(2.2) with an ansatz which does not have a fixed length of spins. The coefficient α determines the degree of the effect of quantum fluctuations. Small value for alpha results huge fluctuations in spin lengths. In numerical calculation, I used two setups with $\alpha = 1$ and $\alpha = 100$. I renormalized the length of the spins with $S = 1$ for the simplicity of calculation. The ansatz I used basically generated from a spiral and a cone phase.

$$\begin{aligned} S_a(\vec{R}) &= S^1_a \cos(\vec{Q}\cdot\vec{R}) + S^2_a \sin(\vec{Q}\cdot\vec{R}) + S^3_a \\ S_b(\vec{R}) &= S^1_b \cos(\vec{Q}\cdot\vec{R}) + S^2_b \sin(\vec{Q}\cdot\vec{R}) + S^3_b \\ S_c(\vec{R}) &= S^1_c \cos(\vec{Q}\cdot\vec{R}) + S^2_c \sin(\vec{Q}\cdot\vec{R}) + S^3_c \end{aligned} \tag{4.1}$$

I calculated the values of free parameters $S^j_i (i = a, b, c; j = 1, 2, 3)$, Q_x and Q_y which minimize the Hamiltonian. The vector $\vec{S^3} = (S^3_a, S^3_b, S^3_c)$ describes the height and the direction of the axis of a cone. $\vec{Q}$ describes the wavevector of the spin wave. In this model, the resulted spin configuration with a magnetic field along the a-axis is identical to the spin configuration appears in the classical model in the previous

section. As illustrated in Figure 4-2, the magnetization along the a-axis, which is represented by S_a^3, is again proportional to B^a. However, in this case the value of S_a^3 exceeds $S(=1)$ and keeps increasing until the energy term of quantum fluctuations grows faster than the decrease of the Zeeman energy. At $h^a = h_{cr}^a$ there is a second

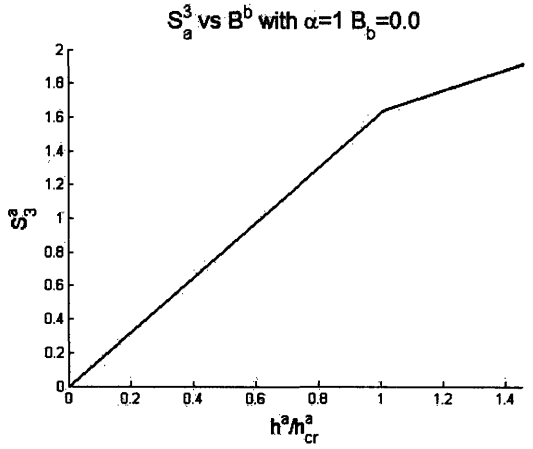

Figure 4-2: The plot of magnetization S_a^3 vs h^a.

order phase transition from the cone state to ferromagnet state. Where the transition happens, there is a kink in the plot of magnetization into a-direction as illustrated in Figure 4-2.

The properties of the ground states with a field along b-axis is more complicated. The plot of the first and second order derivatives of the ground state energy against the magnitude of the applied magnetic field shows that there are two second order phase transitions at $h^b = h_{cr}^b$ and $h^b = 0.23h_{cr}^b$. As it is shown in Figure 4-3, there

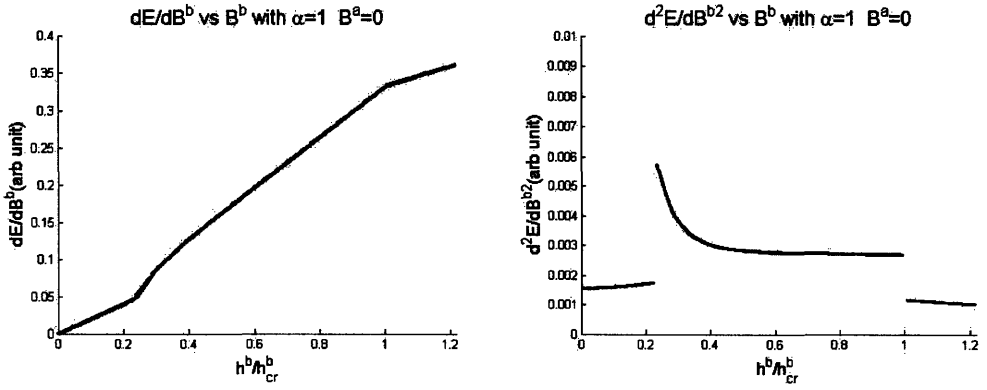

Figure 4-3: the plots of dE/dB^b and $d^2E/d(B^b)^2$ vs h^b.

are two jumps in second order derivatives. To figure out whether the transition point at $h^b = 0.23h^b_{cr}$ is a critical point, the comparison between the plots of the first order derivatives of ground state energy with $h^a = 0$ and $h^a \neq 0$ is needed. The average

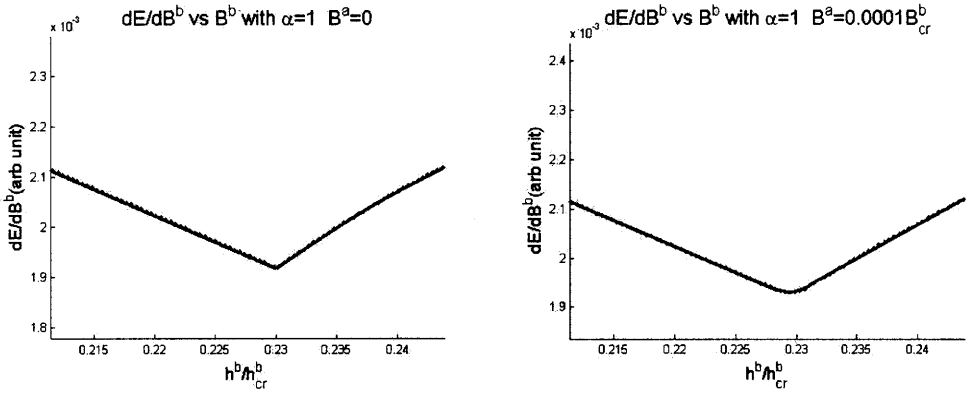

Figure 4-4: the plots of dE/dB^b with $B^a = 0$ and $B^a = 0.0001B^a_{cr}$.

slopes of the plots in Figure 4-4 are reduced for the close look. As it is illustrated in the figure, the kink of dE/dB^b with no field along the a-axis becomes smooth when field along the a-axis is turned on. It shows that the transition point at $h^a = 0$ and $h^b = 0.23h^b_{cr}$ is a critical point.

The result of S^3_a with a magnetic field along the b-axis is described in Figure 4-5. It shows that there is a planar phase in weak field range. As it is described in

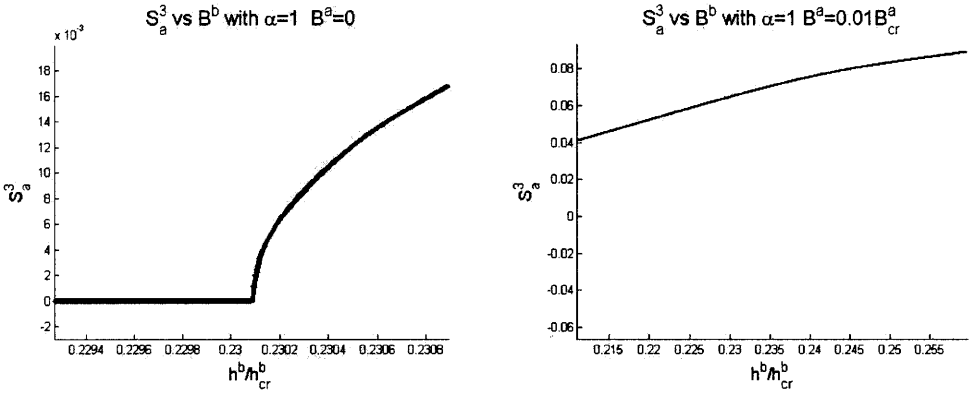

Figure 4-5: (a) The plot S^3_a vs h^b for $h^a = 0$ and (b) the plot S^3_a vs h^b for $h^a = 0.01h^a_{cr}$.

Figure 4-5 (a), a planar phase evolves to a tilted cone state with phase transition at around $h^b/h^b_{cr} = 0.23$. In the planar phase, the collection of spin vectors from each site makes a circle centered at (0,b,0) for non zero b. However, if a magnetic field

has component in a-direction, the planar phase disappears as illustrated in Figure 4-5 (b). In this case, the value of S_a^3 changes smoothly and there is no phase transition.

Following plots in Figure 4-6 shows the different properties between the planar phase and tilted cone phase. Each dots in the plot shows the result of one numerical

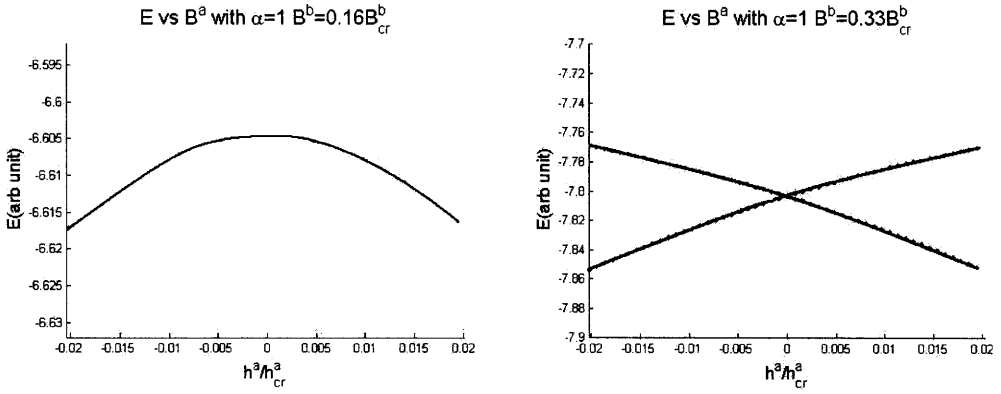

Figure 4-6: (a) The plot of energy versus h^a for $h^b = 0.16h^b_{cr}$ and (b) the plot of energy versus h^a for $h^b = 0.33h^b_{cr}$.

calculations which include many local minima. When points with lowest energies are connected, the curve describing ground state energy is created. There is no crossing lines of energy in (a) for a weak magnetic field where the spin configuration becomes planar at $h^a = 0$. It means there is no phase transition along this line in phase diagram. However, for a intermediate field strength which has tilted cone state for $h^a = 0$, there are two energy states which cross each other at $h^a = 0$, and this means that a first order transition happens on b-axis. When we see the plot of S_a^3 versus h^a, this property can be clearly understood. Two plots in Figure 4-7 shows the change of S_a^3 against a magnetic field in a-axis across the b-axis for two points. The connected solid lines describe the S_a^3 values with ground state energies. The first one shows that when B^a crosses 0 at weak field in b-direction, the tilted angle changes smoothly from positive value to negative value. However, in (b) there is a jump of the values of S_a^3 when B^a changes are made for intermediate B^b where only tilted cone state exists. The discontinuity of S_a^3 is decreased as B^b approaches the critical point where spin configuration transforms into a ferromagnet.

The Figure 4-8 shows the S_a^3 and energy for a strong field $h^b = 1.22h^b_{cr}$ where

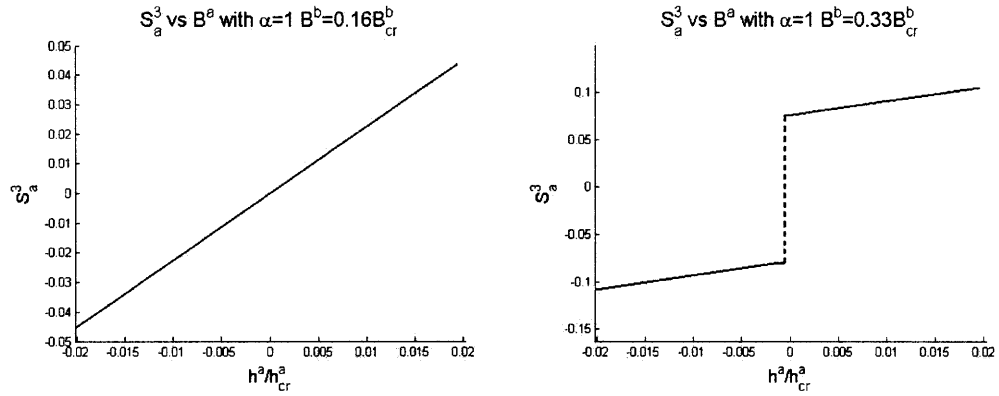

Figure 4-7: (a) The plot of S_a^3 versus h^a for $h^b = 0.16h_{cr}^b$ and (b) the plot of S_a^3 versus h^a for $h^b = 0.33h_{cr}^b$.

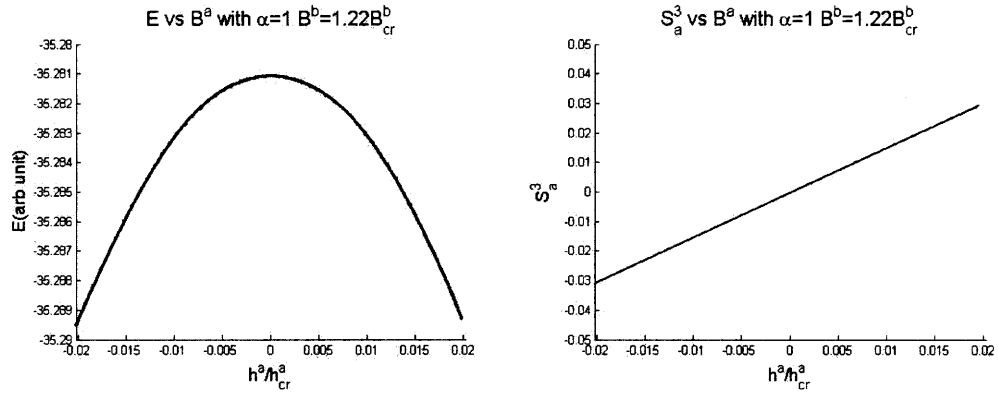

Figure 4-8: (a) The plot of the ground state energy versus h^a and (b)the plot of S_a^3 versus h^a for $h^b = 1.2h_{cr}^b$.

spins lie along the direction of magnetic field. As it is shown in the figure, S_a^3 is proportional to the component of magnetic field in a-axis, and ground state energy changes smoothly. Thus, it can be inferred from the above results that there are first order transition lines along the b-axis for $0.23h_{cr}^b < h^b < h_{cr}^b$. In other words, the first order phase transition across the B^b axis appears for $0.23h_{cr}^b < h^b < h_{cr}^b$.

The plot of ground state energy in Figure 4-9 helps to investigate the characteristics of phase transition at the both ends of the first order phase transition line. As it is appeared in the plot, there are three phases for a field along the b-axis. Point A denotes where planar phase transforms into tilted cone. B indicates the transition point where tilted cone evolves into ferromagnetic phase. The energy splittings in both transition point indicates that both of the phase transitions are second order

transition. The above results can be summarized by the phase diagram shown in Figure 4-10. The dashed line for planar phase indicates that there is no phase transition across the line. The thick solid line in b-axis is a first order transition line and starts from a critical point at $h^b = 0.23h^b_{cr}$. For the case of $alpha = 1$ the ratio h^a_{cr}/h^b_{cr} is almost equal where the reported ratio is 0.95[12]. It is due to the increasing magnetization of the ferromagnet phase for $h^{>}h^a_{cr}$ as explained above. The second order phase transition from ferromagnetic phase to cone or tilted cone phase breaks the translation symmetry. The second order phase transition from the spiral phase to tilted cone phase on B^b axis of the phase diagram breaks the $\mathbb{Z}_2$ symmetry of the spin configuration. Therefore, all of the cone, ferromagnetic and spiral phase have different symmetry properties in their spin configurations. As a result, although our numerical calculation could be applied only for the zero temperature ground state, we can expect that all of these phases appear for a finite temperature condition in real experiments.

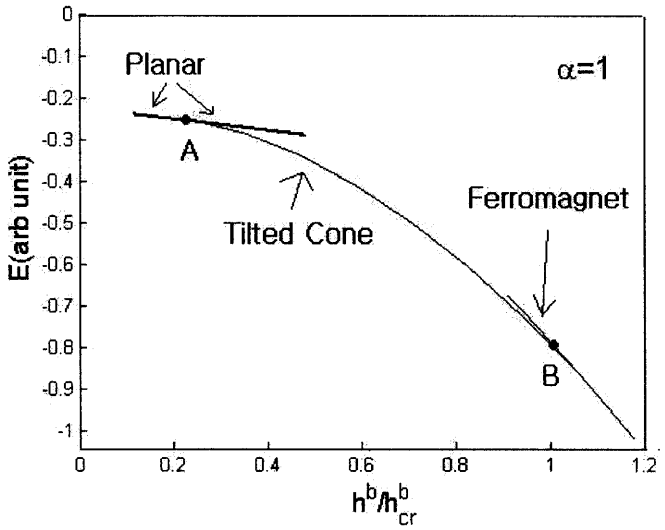

Figure 4-9: The plot of the ground state energy versus B^b for $B^a = 0$

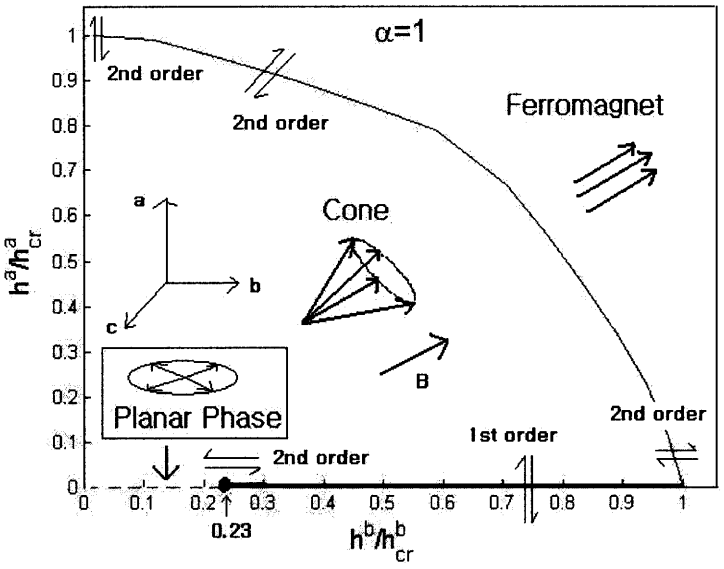

Figure 4-10: B^a-B^b phase diagram of the ground state of Cs_2CuCl_4 derived by numerical calculation with quantum fluctuation effects, $\alpha = 1$

By setting $\alpha = 100$, stronger restriction on quantum fluctuations can be made. With $\alpha = 100$, the second order transition at A of Figure 4-9 appears at weaker field strength. The transition point is about $0.15h^b_{cr}$. Since the effect of quantum

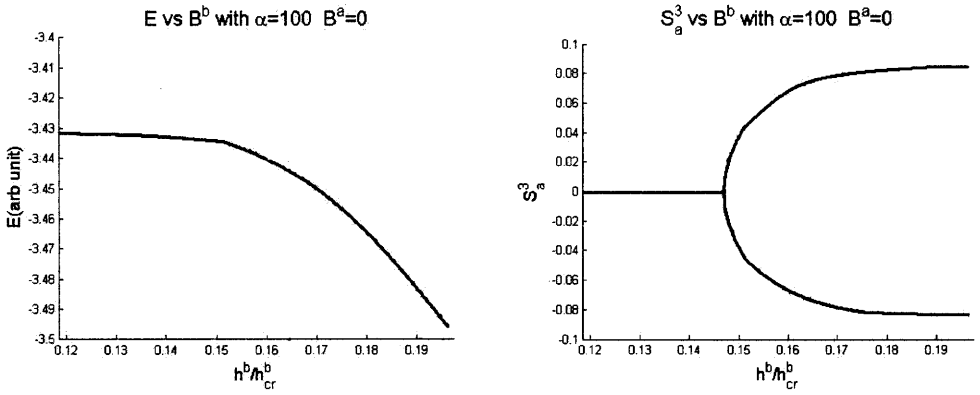

Figure 4-11: (a) The plot of the ground state energy versus B^b for $B^a = 0$, $\alpha = 100$ (b) the plot of the Sz^3 versus B^b for $B^a = 0$, $\alpha = 100$

fluctuation is too small for large α, the center of the circle is very close to the origin. Therefore, $< S_x >$ is nearly zero and the energy of planar phase almost does not change much by B^b. The resulting phase diagram for $\alpha = 100$ is described in Figure 4-12. When this phase diagram is compared with $\alpha = 1$ and the phase diagram of simple

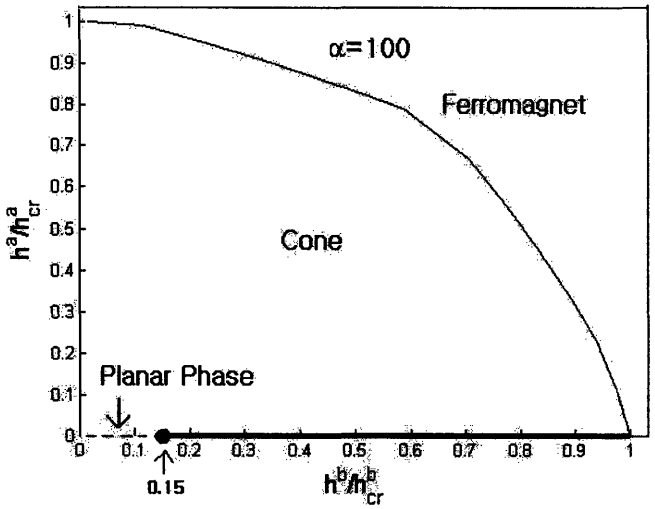

Figure 4-12: B^a-B^b phase diagram of the ground state of Cs_2CuCl_4 derived by numerical calculation with quantum fluctuation effects, $\alpha = 100$

classical model in previous section, it is reasonable to have smaller range of planar phase for smaller quantum fluctuations on spin length, given by large α.

4.3 Order Parameter

The phase diagram of the ground state of Cs_2CuCl_4 in B^a and B^b can be understood by two order parameters $\vec{n}$ and $\cos\theta$ with potential U given by,

$$U = a\cos^2\theta - b(n_a B^a + n_b B^b)\cos\theta + c(n_b^2 + n_c^2) + d(n_b^2 + n_c^2)^2 \qquad (4.2)$$

where $\vec{n}$ is a unit vector which indicate the direction of the axis of a cone which consists of spins in each site. $\cos\theta$ denotes the height of the cone. Since the magnetic field used in numerical calculation has no unit, we can renormalize the field strength as $B' = B/B^a_{cr}$ where B^a_{cr} is the transition point between the cone phase and ferromagnet with a field along a-axis. In this unit, B^b_{cr} is also 1.00.

The ratios between coefficients can be derived from the location of phase transitions. Since the minimization of the potential function requires $n_c = 0$, U can be

simplified as follow by setting a=1.

$$U = \cos^2\theta - b(n_a B^a + n_b B^b)\cos\theta + cn_b^2 + dn_b^4 \tag{4.3}$$

When $B^b = 0$, potential function has its minimum value for $\cos\theta = \frac{b_1 B^a}{2}$. Using the fact that $\cos\theta = 1$ at $B^a = 1$, b is 2.

For $B\|\hat{b}$, U becomes a function of two order parameters n_b and $\cos\theta$.

$$U = \cos^2\theta - bn_b B^b\cos\theta + cn_b^2 + dn_b^4 \tag{4.4}$$

This function has minimum value at $n_b = 0$ when $(\frac{bB^b}{2})^2$ is less than c. Using that n_b is zero for $B^b < 0.23 B_{cr}^b = 0.23$ with $\alpha = 1$, the value of c is determined as 0.053. For large B^b, minimization of U for $\cos\theta$ gives,

$$n_b = \sqrt{\frac{1}{4d}(-2c + \frac{(bB^b)^2}{2})} \tag{4.5}$$

Since n_b is 1 when $B^b = B_{cr}^b = 1$, d is 0.69. Therefore, the potential as a function of $\cos\theta$ and n_b for a field in a-b plane,

$$U = \cos^2\theta - 2(\sqrt{1 - n_b^2}B^a + n_b B^b)\cos\theta + 0.053n_b^2 + 0.69n_b^4 \tag{4.6}$$

The interpretation of each terms in the potential function can be made by comparing to the original Hamiltonian. The length of a spin in b-c plane is proportional to $\sin^2\theta = 1 - \cos^2\theta$. Therefore, the first term describes the energy from exchange interactions. The second term represent the Zeeman energy. The third and fourth term requires n_b and n_c be small which means they prefer spins on b-c plane. Thus, these terms describes the effect of DM interaction with small coefficient. The potential function in equation (4.6) predicts that in the boundary of tilted cone phase,

$$n_a B^a + n_b B^b = \cos\theta = 1. \tag{4.7}$$

This condition suggests a ferromagnet phase where spins lie along the direction of $\vec{n} = (B^a, B^b, 0)$.

Chapter 5

Conclusion

In this paper, I studied the spin configuration of the ground state of Cs_2CuCl_4 in the presence of magnetic field. The numerical result for the spin configuration with a magnetic field along the a-axis consists of a cone phase for low field and ferromagnetic phase for high field which agrees with the experimental result. Ground state with longitudinal field has three phases which are separated by second order phase transitions. For weak field of $h^b < 0.23h^b_{cr}$, the spiral planar phase appears. However, the phase appears with our model is not a distorted cycloid but a circle with a slight shift of center into the direction of field. For intermediate field range, $0.23 < h^b/h^b_{cr} < 1$, the tilted out of plane cone phase appears and breaks the $\mathbb{Z}_2$ symmetry. The phase with no long range order which appeared in previous experiments did not appear in this model. For high field of $h^b_{cr} < h^b$, ferromagnetic phase appears. In the presence of both of longitudinal and transverse field, the spin configuration is a tilted cone for a low field and becomes a ferromagnetic phase for a high field. The phase transition between these two states is a second order transition. This result can be compared to [13]. In [13], the transition between a distorted cycloid phase and phase for the intermediate field is a first order transition. However, the numerical calculation presented in this paper shows slightly different features. This difference is due to the neglecting the interlayer interaction and newly added term in our Hamiltonian which represents the quantum fluctuation effect. It will be also interesting to investigate the spin configuration with longitudinal magnetic field with a new Hamiltonian with

additional terms which breaks U(1) symmetry since the experimental result shows different phase diagrams for two longitudinal field directions b and c. Moreover, the numerical calculation with those additional terms and interlayer exchange interactions will be helpful to understand the real magnetic phase diagram.

Bibliography

[1] P. W. Anderson. *Master. Res. Bull. 8, 153*, 1973.

[2] S. Bailleul, J. Holsa, and P. Porcher. *Eur. J. Solid State Inorg. Chem. 31, 432*, 1994.

[3] C. H. Chung, J. B. Marston, and R. H. McKenzie. *J. Phys. : Condens. Matter 13, 5159*, 2001.

[4] C. H. Chung, K. Voelker, and Y. B. Kim. *Phy. Rev. B 68, 094412*, 2003.

[5] R. Coldea, D. A. Tennant, R. A. Cowley, D. F. McMorrow, B. Dorner, and Z. Tylczynski. *J. Phys. Condens. Matter 8,7473*, 1996.

[6] R. Coldea, D. A. Tennant, K. Habicht, P. Smeibidl, C. Wolters, and Z. Tylczynski. *Phys. Rev. Lett. 88, 137203*, 2002.

[7] R. Coldea, D. A. Tennant, A. M. Tsvelik, and Z. Tylczynski. *Phys. Rev. Lett. 86, 1335*, 2001.

[8] R. Coldea, D. A. Tennant, and Z. Tylczynski. *Phys. Rev. B 68, 134424*, 2003.

[9] I. Dzyaloshinskii. *J. Phys. Chem. Solids 4, 241*, 1958.

[10] J. O. Fjaerestad et al. *cond-mat/0701014*, 2007.

[11] T. Moriya. *Phys. Rev. 120, 91*, 1960.

[12] Y. Tokiwa, T. Radu, R. Coldea, H Wihelm, Z. Tylczynski, and F. Steglich. *cond-mat/0601272*, 2007.

[13] M. Y. Veillette, J. T. Chalker, and R. Coldea. *cond-mat/0501347*, 2007.

[14] Y. Zhou and X. G. Wen. *cond-mat/0210662*, 2008.